

# A search for transit timing variations within the exomoon corridor using *Kepler* data

David Kipping<sup>1\*</sup> and Daniel A.. Yahalom<sup>1</sup>

<sup>1</sup>Dept. of Astronomy, Columbia University, 550 W 120th Street, New York NY 10027

Accepted 2022 November 10. Received 2022 November 10; in original form 2022 August 31

## ABSTRACT

An exomoon will produce transit timing variations (TTVs) upon the parent planet and their undersampled nature causes half of such TTVs to manifest within a frequency range of 2 to 4 cycles, irrespective of exomoon demographics. Here, we search through published *Kepler* TTV data for such signals, applying a battery of significance and robustness checks, plus independent light curve analyses for candidate signals. Using the original transit times, we identify 11 (ostensibly) single-planets with a robust, significant and fast ( $P_{\text{TTV}} < 4$  cycles) TTV signal. However, of these, only 5 are recovered in an independent analysis of the original photometry, underscoring the importance of such checks. The surviving signals are subjected to an additional trifecta of statistical tests to ensure signal significance, predictive capability and consistency with an exomoon. KOI-3678.01, previously validated as Kepler-1513b, is the only case that passes every test, exhibiting a highly significant ( $> 20\sigma$ ) TTV signal with a periodicity, amplitude and shape consistent with that caused by an exomoon. Our analysis finds that this planet is  $8.2^{+0.7}_{-0.5} R_{\oplus}$  orbiting at  $0.53^{+0.04}_{-0.03}$  AU around a late G-type dwarf. After forecasting the planetary mass, we expect it to be capable of maintaining at least a  $0.3 M_{\oplus}$  exomoon for 5 Gyr, and the TTV signal corresponds to a moon mass as low as 0.75 Lunar masses. We thus encourage follow-up observations and dynamical analysis of this unique signal, but caution skepticism until such data can be obtained.

**Key words:** planets and satellites: detection — methods: data analysis — techniques: photometric

## 1 INTRODUCTION

The Solar System reveals that moons appear to be a natural by-product of planet formation. Indeed, at least three distinct mechanisms appear required to explain the largest moons (0.2–0.4  $R_{\oplus}$ ); a capture mechanism for Triton (e.g. see Agnor & Hamilton 2006), a giant impact for the Moon (Reginald 1946) and in-situ formation disk (e.g. see Canup & Ward 2002). If transiting exoplanets possess moons, then they should be expected to also transit, as well as perturb the path of the parent planet such as via TTVs, transit timing variations (Sartoretti & Schneider 1999). Whilst the detection of both effects is ultimately sought, yielding a radius and mass respectively, the two effects will in general have different signal-to-noise ratios (SNRs), meaning that for observations at the threshold of detectability, we should only expect one to be initially found.

To date, there is only one known example where both signatures appear to manifest - Kepler-1625b-i (Teachey & Kipping 2018). Although the TTV signal here appears ro-

bust, the moon transit was independently recovered by one team (Heller, Rodenbeck, & Bruno 2019) but not another<sup>1</sup> (Kreidberg, Luger, & Bedell 2019) – thus leaving the situation ambiguous without follow-up observations. Extensive searches for additional moon-like transits have been attempted (e.g. see Kipping et al. 2012 and subsequent papers in that series) but only one other *Kepler* candidate has been reported to exhibit such a signature, the exomoon candidate Kepler-1708b-i (Kipping et al. 2022). In that case the TTV is presently undetectable since only two epochs have been observed to date.

Despite the considerable focus on moon transits, TTVs were amongst the first methods proposed to look for exomoons (Sartoretti & Schneider 1999), have been catalogued for hundreds of systems (e.g. Mazeh et al. 2013) and dozens of confirmed TTV systems now exist thanks to their planet-planet interactions (e.g. Hadden & Lithwick 2014). The clas-

\* E-mail: dkipping@astro.columbia.edu

<sup>1</sup> However, a comparative study of the different light curve reductions indicated that the reduction of Kreidberg, Luger, & Bedell (2019) appeared to be affected by systematics.

## 2 Kipping & Yahalom

sic problem with TTVs is indeed this latter point though, how can one discern whether a given TTV signal is due to an exomoon or a perturbing planet? Transit duration variations (TDVs) can break this degeneracy in ideal conditions (Kipping 2009a), but in practice TDV measurements are rarely precise enough to tease out these effects. Radial velocity (RV) measurements could also come to the rescue, by eliminating the hidden planet hypothesis, but here too sufficiently precise RV measurements of the faint *Kepler* stars have been lacking for the majority of planets. One recently highlighted “statistical” answer is to look at the TTV frequency.

This idea was described in Kipping (2021), where it was shown that exomoon induced TTVs will always be undersampled and thus their signatures will manifest as aliases. These aliases are much more likely to occur close to the Nyquist frequency and in fact 50% of all of these aliases will occur in a period range of 2-4 cycles; the so-called “exomoon corridor”. What’s remarkable is that this result is independent of the exomoon population properties, and is distinctive from the typically much longer periodicities planet-planet interactions produce Hadden & Lithwick (2014).

Pulling on this thread, we here conduct a search for TTV signals in the exomoon corridor. We start with the Holczer et al. (2016) catalog (H+16 hereafter), derived from the *Kepler* data, as our initial input, which is then filtered down to the most exomoon-like signatures in Section 2. We then independently analyse the light curves of the best candidates to confirm their candidacy in Section 3. We discuss our only surviving candidate in Section 4 before highlighting broader implications of this work in Section 5.

## 2 FILTERING OF THE H+16 CATALOG

Our analysis makes use of the H+16 transit timing catalog derived from the *Kepler Mission*. Despite being published six years ago, H+16 remains the most up-to-date dedicated public *Kepler* TTV catalog at the time of writing. H+16 report that on 23rd November 2013, 4690 KOIs were listed in the NASA Exoplanet Archive after eliminating false positives, whereas on 19th July 2022 that number is marginally higher at 4716. A large number of KOIs were deemed unsuitable for TTV analysis by H+16, for having insignificant depths, excessively large depths, periods greater than 300 days, or for being a known false alarm/eclipsing binary. After these cuts, 2599 KOIs were used to produce the H+16 TTV catalog.

We note that many of the KOIs that H+16 ignored can be filled in using the transit times available from Rowe et al. (2014) and Rowe & Thompson (2015). However, by virtue of H+16’s filters, these are inherently lower quality KOIs to work with, and would also lead to a non-homogeneous input catalog. For these reasons, we elect to not include them here.

H+16 produced a summary list of KOIs which they concluded to have a significant ( $p$ -value  $< 10^{-4}$ ), long-term ( $P_{\text{TTV}} > 100$  days) TTV signal (their Table 5), and also another list of those with a significant, short-term ( $3 < P_{\text{TTV}} < 80$  days) TTV signal (their Table 7). A scoring system that rests primarily on  $p$ -values is somewhat precarious as it truly only ranks the “surprisingness” of an event, and is commonly misinterpreted to equate to the probability that the null hypothesis (i.e. “there is no TTV”) is true (Colquhoun 2014;

Wasserstein & Lazar 2016). Certainly such cases are deserving of further attention, but in isolation an extreme  $p$ -value leaves room for ambiguity about the reality of the putative signal. Further, the short/long-term definitions used by H+16 are framed in terms of absolute temporal units (i.e.  $P_{\text{TTV}}$ ), whereas the exomoon corridor we seek is defined on a relative temporal scale (i.e.  $P_{\text{TTV}}/P$ ).

We also note that Kane et al. (2019) produced an independent visual ranking of TTV systems, leveraging the H+16 catalog as well as that of Rowe et al. (2014) and Rowe & Thompson (2015). Whilst we will compare our results to earlier work at the end, we elected to conduct our own selection procedure for significant TTVs that focusses more on inferential statistical measures, and only utilizes  $p$ -values for flagging *potentially* spurious cases, rather than flagging candidate TTV detections.

### 2.1 Lomb-Scargle periodograms

In searching for an exomoon corridor signal, we highlight two key features that affect our strategy: i) an exomoon TTV signal is expected to be strictly periodic (Sartoretti & Schneider 1999; Kipping 2009a), and ii) the transit timing catalog from H+16 is often sparse. Accordingly, periodic signals should be sought using a Lomb-Scargle (LS) periodogram (Lomb 1976; Scargle 1982).

Crucially, we highlight that the LS periodogram is ideally run on the transit times, not the TTVs. By definition, TTVs are the transit times with a linear ephemeris subtracted, and that linear ephemeris must have been derived from a regression of effectively the transit times (at least with this data set). In principle, there’s no reason why one can’t indeed do two regressions of the transit times; one that derives the linear ephemeris, and then a separate second one that fits a periodic signal through the TTVs. However, such a two-stage process does not trivially propagate the uncertainty of the linear ephemeris itself into the inference of the periodic signal<sup>2</sup>. This could be accommodated by utilising the covariance function derived from the linear ephemeris, but it’s far simpler and more robust to just fit the transit times directly to a linear ephemeris plus sinusoidal model.

Accordingly, our LS periodogram defines a grid of trial periods and then at each period regresses two models to the H+16 transit times. The null model is simply:

$$\tau_{\text{null},e} = P_{\text{null}} * e + \tau_{\text{null,ref}}, \quad (1)$$

where  $e$  is the epoch number,  $P$  is the planetary period,  $\tau$  is the time of transit minimum and the subscripts “null” and “ref” refer to the null hypothesis model and the reference epoch respectively. The second model we regress is that of a linear ephemeris with a sinusoidal variation added on top:

$$\tau_{\text{sin},e} = P_{\text{sin}} * e + \tau_{\text{sin,ref}} + a_S \sin(n_{\text{TTV}}e) + a_C \cos(n_{\text{TTV}}e), \quad (2)$$

where  $n_{\text{TTV}}$  is the trial frequency ( $\equiv 2\pi/P_{\text{TTV}}$ ), and  $a_S$  and  $a_C$  are the two linear amplitude components of a sinusoidal wave. By writing the model out this way, and working

<sup>2</sup> Indeed said error propagation is not conducted in the analysis of H+16.

along a pre-defined frequency grid, the problem is linear with respect to the unknown parameters and thus we exploit a linear solver to infer the best-fitting model.

Outlier transit times can significantly distort the results of an LS periodogram, which is predicated upon mean-based (weighted linear least squares) statistics. To alleviate this somewhat, we apply a simple outlier rejection scheme to the H+16 transit times. To this end, we first extract the quoted TTVs from H+16 and divide them by their quoted uncertainties. We next measure the RMS of this list using a median-based robust measure, specifically 1.4826 multiplied by the median absolute deviation (MAD). We then remove any transit times for which the quoted TTV normalised by the quoted uncertainty exceeds 10 times this robust RMS value. The idea here is to reject points which are dispersed an order-of-magnitude more than the observed scatter. We also remove any transit times for which the H+16 reported uncertainty is  $> 3$  times greater than the median uncertainty of that KOI, typically associated with partial transits of poorer data quality.

For the period grid, we define the shortest period using the Nyquist rate (Nyquist 1928), which is given by the twice the minimum temporal spacing between any two transit times (almost always 2 cycles). The longest period is given by twice the temporal baseline of the transit times. In principle, the number of periods/frequencies scanned should be equal to the number of transit times (VanderPlas 2018), but in practice we overscan by a factor of ten to create a smooth, dense periodogram. At each period, we evaluate the  $\chi^2$  of two competing models, which are then appended and saved to disk. We also save the amplitude of the best fitting TTV signal ( $= \sqrt{a_s^2 + a_c^2}$ ), the number of available transit times, and finally a modification of the  $\chi^2$  metric using median statistics that we dub  $\Xi^2 = n \text{median}[(\mathbf{r}/\sigma)^2]$ .

After this effort, we are now ready to apply our first filter to the H+16 catalog. Specifically, we cut down to KOIs for which the peak  $P_{\text{TTV}}$  (as derived from our LS periodogram) is less than 20 cycles (the  $\simeq 95\%$  confidence limit of the exomoon corridor; Kipping 2021) and the Bayesian Information Criterion (BIC; Schwarz 1978) favours the sinusoidal model. This first filter can be thought of as a “rough cut” for potentially interesting exomoon corridor signals. The filter reduces the number of KOIs from 2599 to 1822. Thus, taking the H+16 transit times at face value, there is a very large number of KOIs which seemingly exhibit evidence (or at least “a statistical preference”) for periodic TTVs<sup>3</sup>.

## 2.2 Remove false positives and multis

On 26th December 2021, we downloaded the NEA and flagged any KOIs for which either the “Exoplanet Archive Disposition” or the “Disposition Using Kepler Data” columns listed “FALSE POSITIVE”. All such KOIs were removed from our sample. At the same time, we also remove any KOIs residing a multi-system. The justification for this is simply that single-planet systems exhibiting TTVs demand additional mass in the system to explain the data,

whereas multi-planet data does not necessarily. For this reason, we consider single-planet TTVs more interesting (for our purposes) than multis. Applying these two criteria reduce the sample from 1822 KOIs to 917. Figure 1 shows the TTV amplitudes versus orbital periods of the sample before and after applying this cut, to visualise how the population is sculpted by this filter (as well as subsequent filters in this section).

## 2.3 Remove TTVs above the exomoon ceiling

For our third filter, we exploit the “impossible moons” argument of Kipping & Teachey (2020). In that work, it is shown that exomoons that are bound to be i) within the Hill sphere of the their parent planet, and ii) less massive than their parent planet, will have a well-defined maximum possible TTV amplitude. Thus, any TTV amplitudes observed above this ceiling must be non-exomoon in nature.

To calculate the ceiling, we first take the NEA reported maximum *a-posteriori* (MAP) ratio-of-radii (primarily sourced from the DR25 analysis of Thompson et al. (2018)) and multiply by it by the MAP stellar radius reported in the homogeneous stellar catalog of Berger et al. (2020). These planetary radii are converted to a low- and high-estimate of the planetary mass using a modified version of `forecaster` (Chen & Kipping 2017). Specifically, since here we only need a point-estimate, we take the deterministic form of `forecaster` to express  $R_P(M_P)$  up to the Neptunian-Jovian transition point of  $131.6 M_\oplus$ . Since the equation is monotonic up to here, one can simply invert  $M_P(R_P)$ . Beyond this transition, the relation become degenerate and so we make two extreme assumptions about the planetary mass - it is either fixed to  $131.6 M_\oplus$  (a Saturnian low-ball estimate) or to the mass corresponding to the Jovian-stellar transition at  $0.08 M_\odot$  (a brown dwarf high-ball estimate). With this, we are able to convert the reported radii to masses, giving two extrema values for the Jovian-sized worlds.

Equipped with a planetary mass, we can now estimate the maximum stable exomoon mass using Equation (9) of Barnes & O’Brien (2002) - which considers the tidal migration of a moon around a planet. This is technically done twice, for the low- and high- mass estimates (although these estimates are identical for sub-Jovian planets), and where all other parameters are kept consistent from before (e.g. the Berger et al. (2020) stellar parameters are used). This expression also requires an estimate for the tidal value ( $k_{2p}/Q_P$ ), which is interpolated based off the Solar System empirical  $R-(k_{2p}/Q_P)$  relation following Teachey, Kipping, & Schmitt (2018) (see their Figure 1). We then compute the corresponding TTV amplitude of the system using the model of Kipping (2009a) and compare the value to the amplitude found from the peak of the LS periodogram. If the observed amplitude exceeds the ceiling, as derived using *either* of the low-/high-ball mass estimates, then the KOI is rejected as a plausible exomoon signal. This filter reduces our sample down from 917 KOIs to 314.

## 2.4 Robustness test of the statistical preference

In test 1, each signal was filtered to have a statistical preference for a periodic TTV rather than a linear ephemeris.

<sup>3</sup> A similar result was also reported by Kipping & Teachey (2020).

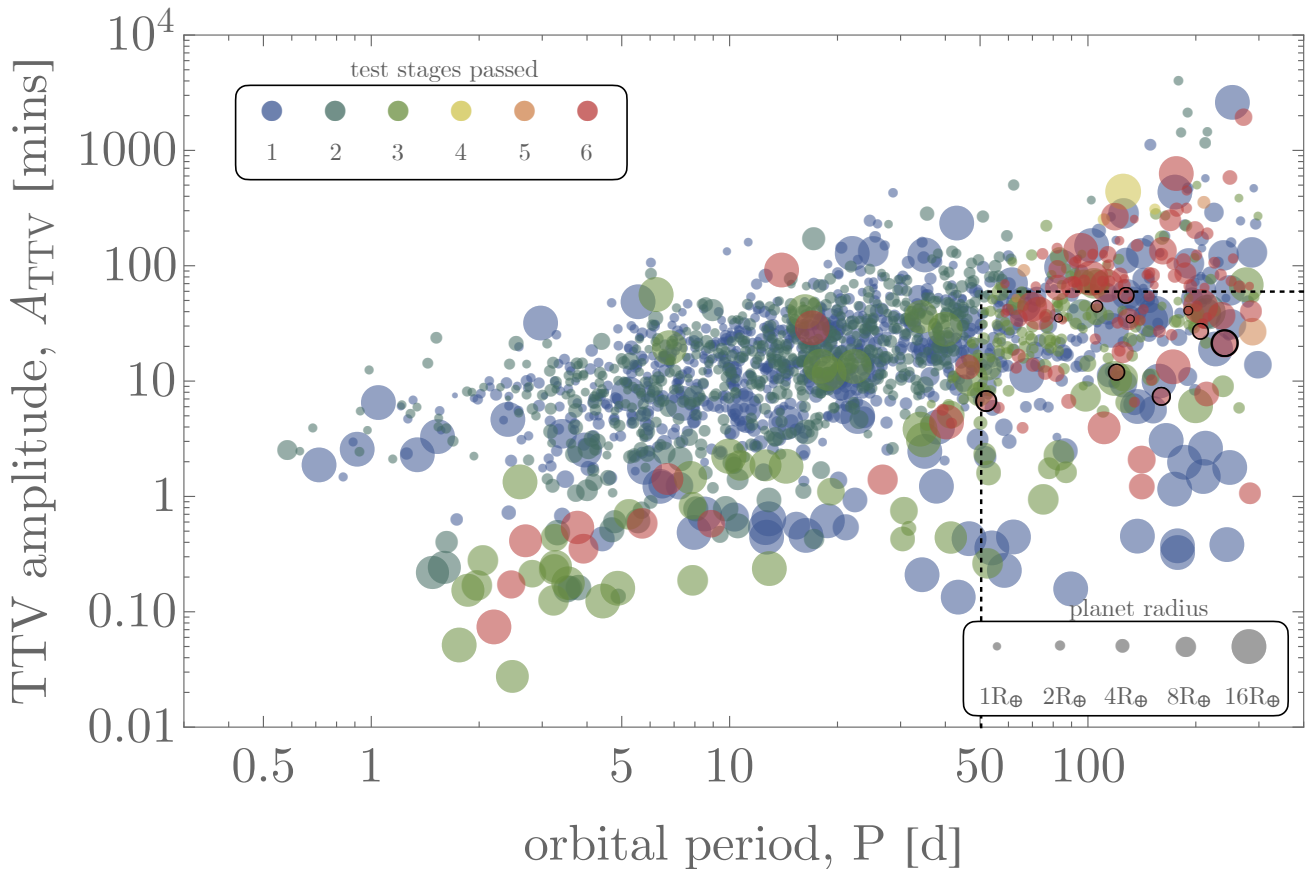


**Figure 1.** 1822 KOIs for which we identify a  $\Delta\text{BIC} > 0$  periodic TTV signal of less than 20 cycles periodicity using the H+16 transit timing catalog (with outlier rejection preconditioning applied). The different colored point show the survivors from various test stages applied in Section 2, where the population drops from  $1822 \rightarrow 917 \rightarrow 314 \rightarrow 129 \rightarrow 126 \rightarrow 122$  (blue to red) in applying the various tests. The final 22 used in Section 3 are highlighted with black circles.

That test was conducted using the BIC metric, but in isolation that metric can be misleading; in particular because of the possible presence of outliers or additional stochastic noise not captured by the formal TTV uncertainties. Although some outlier rejection was applied during the LS periodogram (see Section 2.1), it is possible outliers several times greater than the TTV scatter could persist.

To address this, we here employ a fourth filter, which ensures the statistical preference is robust against these possibilities. To check against a single dominant outlier, we iteratively dropped out a TTV point from the time series and repeat the sinusoidal fit at the putative period. Cycling through all possible permutations, we demand that the BIC on these truncated time series always favours the periodic model. In this way, our claim for statistical preference is robust against any one single point being an outlier.

A possible weakness of this test is that it truly only tests for robustness against a single outlier, but multiple outliers could also deceive us into claiming a spurious signal. Accordingly, we also demand that the  $\Xi^2$  of the sinusoidal fit residuals are lower than that of the linear ephemeris. As noted earlier (see Section 2.1), this is a median-based version of the  $\chi^2$  and thus remains robust up to a <50% contamination fraction from outliers.

Another possibility is that there are no outlier per se,

but that the timing uncertainties are globally underestimated. As an example, starspots can induce spurious TTVs (Ioannidis, Huber, & Schmitt 2016) that would not be captured by the formal uncertainties of H+16, since they did not employ a spot model in their inference. As a test for this, let us assume that the periodic model is correct but that the errors are too small. In that case, we would expect the  $\chi^2$  of the periodic model with correctly adjusted uncertainties to approximately equal the number of degrees of freedom. We thus scale the errors to satisfy this condition<sup>4</sup> and then recompute the  $\Delta\text{BIC}$  between the two competing models. Robust models should still have a preference for the periodic model even after this rescaling.

Of the 314 remaining KOIs, 186 passed the drop-out test, 239 pass the  $\Xi^2$  test and 243 pass the rescaling test. Applying all three together reduces our sample of 314 KOIs to 129. To illustrate these tests in action, Figure 2 shows three cases where just one of these tests were failed (KOIs-633.01, 1535.01, 1876.01), and a fourth case where all tests were passed (KOI-92.01).

<sup>4</sup> We also impose that this scaling factor cannot be less than unity (i.e. we never shrink the formal uncertainties).

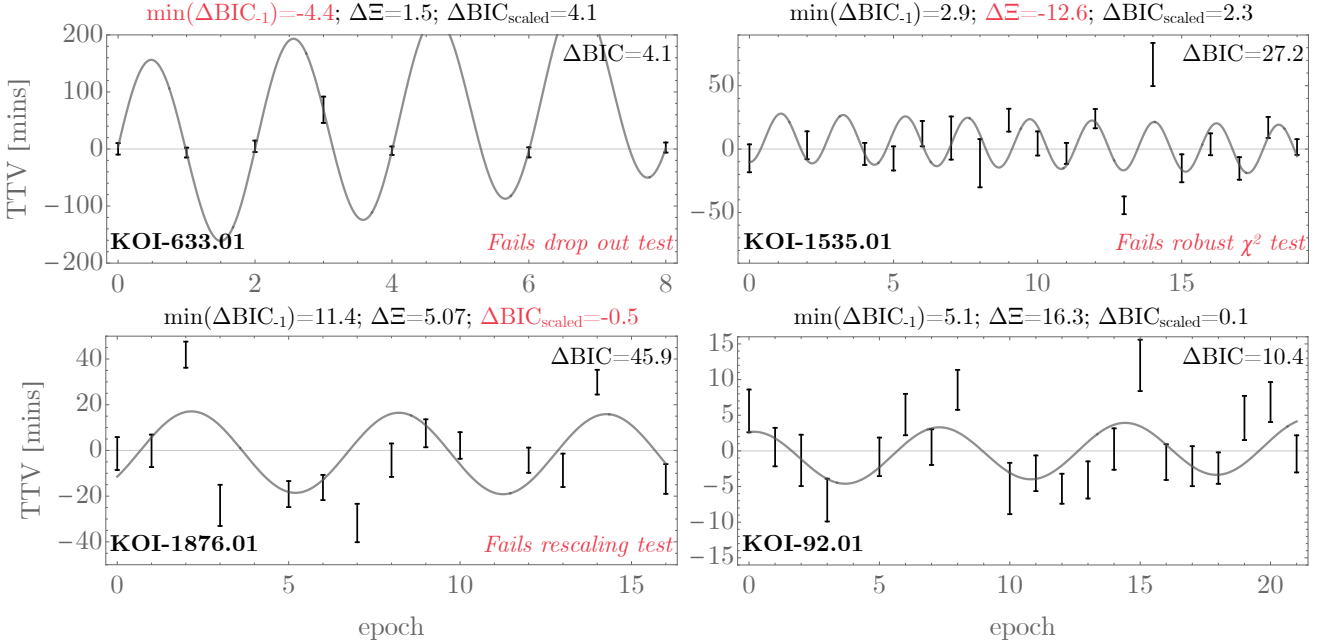


**Figure 2.** Top-left, top-right and lower-left panels show three examples of TTVs derived from the H+16 the transit times that fail our significance robustness tests. Each case highlights in red the specific test that was failed. The lower-right panel shows an example of a KOI that passes all tests. Each panel includes the best-fitting sinusoidal signal as derived from a LS periodogram search.

## 2.5 Test for suspicious phase clustering

For a given KOI, one can fold the TTVs upon the peak period derived from LS periodogram and inspect the distribution of the resulting phase-folded TTVs. In general, there is no reason why a real signal would feature clustering in phase-space, but this could be consistent with a spurious signal. This can occur if the candidate period lies close to an aliasing of the window function, leading to a chopping effect in the sampling. Such suspicious cases can be flagged by simply phase-folding the TTVs upon the best period and employing the classic Kolmogorov-Smirnov (KS) test (Kolmogorov 1933; Smirnov 1948). We evaluate the  $p$ -value from the KS test against a uniform distribution to flag KOIs with surprising phase distributions. This test results in just three suspicious cases ( $p < 0.05$ ), including KOI-5942.01 which we highlight as an example in Figure 3. With these three KOIs dropped, we are left with 126 KOIs.

## 2.6 Test for adequate phase coverage

Along the same lines, the phase clustering could be quasi-uniform but have poor coverage in the phase-folded space. To quantify this, we define a ‘‘coverage metric’’,  $C$ , which is equal to the difference between the maximum and minimum phase-folded TTV phase. Small  $C$  values are clearly suspicious, implying the observed TTVs only span a relatively small fraction of the supposed signal.

To identify surprisingly low  $C$  values more rigorously, for each KOI we took the TTVs and folded them upon a random frequency uniformly distributed between the minimum and maximum periods used in our LS periodogram search. After folding, we measure the  $C$  metric and then repeat until 1000

such samples have been generated. We then evaluate the  $p$ -value of the real  $C$  score by comparing to this distribution.

Four KOIs were found to have suspiciously low  $C$  scores ( $p < 0.05$ ), with the example of KOI-2177.01 shown in Figure 3. KOI-2177.01 is particularly interesting to highlight because inspection of the phase folded TTVs reveals a clearly spurious signal, but one that unexpectedly passed the previous phase distribution test. Indeed, with the phase distribution test, the  $p$ -value of the KS test against a uniform distribution was 0.081, but with the coverage test it finally gets flagged with  $p = 0.017$ . Such cases highlight that no battery of tests is perfect, but in unison a large number of spurious cases can be trimmed, saving timing in the later analyses. With these four KOIs removed, we are left 122 KOIs.

## 2.7 Final downsampling

For our final downsampling, we more aggressively hone in on potentially significant, highly-exomoon like signals. To this end, we apply a much stronger statistical cut that  $\Delta(\text{BIC}) > 10$  and only accept exomoon corridor KOIs such that  $P_{\text{TTV}} < 4$  cycles (corresponding to the 50th percentile of expected exomoon periods; Kipping 2021). We also eliminate any signals with TTV amplitudes in excess of one hour,  $\leq 4$  available epochs and planets with periods less than 50 days. We find that 11 of the 122 KOIs fall within this range and define our H+16 exomoon-like TTV candidates.

We note that 120 of the 122 satisfy our revised statistical threshold, which is perhaps not surprising given the battery of robustness tests such signals have thus far survived. However, we caution against treating these as ‘‘detections’’ in the absence of an independent light curve analysis. For as the next section will show, most of our 11 exomoon

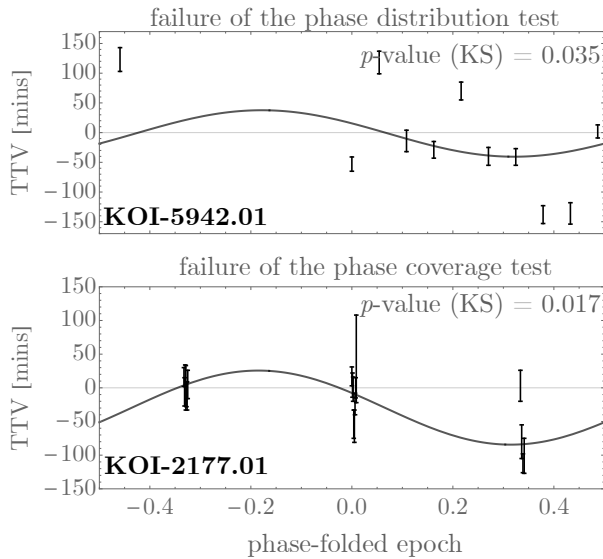


**Figure 3.** Top: an example of a TTV signal that fails our test for uniform phase coverage. After phase-folding upon the candidate TTV period, the TTVs are disproportionately occurring in the second-half of the diagram. Lower: an example of a TTV signal that fails our phase coverage test. Given the generous number of points, it’s highly unlikely the phase-folded TTVs would only span  $\sim 70\%$  of the available window, and visual inspection confirms the spurious nature of this signal. In both cases, the blue line shows the fitted candidate TTV signal.

corridor candidates do not survive an independent analysis. This final subset is highlighted with black circles in Figure 1, and are listed in Table 1 (although KOI-5825.01 is excluded since our later fits are unable to constrain its transit times, see Section 3.4).

### 3 INDEPENDENT ANALYSES OF THE SURVIVORS

Having identified KOIs that appear to have significant TTV signals within the exomoon corridor based upon the H+16 catalog, we next challenge the veracity of that claim through an independent light curve analysis.

#### 3.1 Light curve detrending

We begin by performing an independent light curve detrending of the *Kepler* time series photometry; specifically here we use the long-cadence (LC) data. The light curve treatment is almost identical to that of Kipping et al. (2022) and so we direct the reader there for details. In brief, the light curves are detrended on an epoch-by-epoch basis using four distinct algorithms (`cofiam`, `polyam`, `local` and `gp`) applied to two distinct data products (SAP and PDC). For each transit of each KOI, this produces eight light curves which are then tested to see if they behave consistently with Gaussian noise, and if so are then combined together through “method marginalisation”. This final stage takes the median of the  $\leq 8$  photometric points at each time stamp, and propagates a robust standard deviation estimate between them

into the formal uncertainties. The final method marginalised light curves are used for fitting.

The only difference between our treatment here and that of Kipping et al. (2022) is that the H+16 transit times are used (where available) to define the mid-point of each epoch. This is helpful since all algorithms need to mask the transit signal, which of course depends upon the temporal location of the transit.

#### 3.2 Light curve fits

For each KOI, two models are regressed to the detrended data. Model  $\mathcal{P}$  assumes a linear ephemeris for the planet whereas model  $\mathcal{T}$  assumes each epoch has a unique time of transit minimum,  $\tau_e$ . Both models use the Mandel & Agol (2002) algorithm, combined with the Danby (1988) solver for the Kepler equation, numerical resampling of the finite integration time following the method of Kipping (2010) and the re-parameterised quadratic limb darkening coefficients of Kipping (2013).

The regression was performed using the multimodal nested sampling code `MultiNest` (Feroz, Hobson, & Bridges 2009) using 4000 live points. Our fits adopted a uniform prior for the ratio-of-radii,  $p$ , between 0 and 1, a uniform prior for the impact parameter,  $b$ , between 0 and 1, a log-uniform prior for stellar density,  $\rho_*$ , between  $10^{-3} \text{ g cm}^3$  to  $10^{+3} \text{ g cm}^3$ , a uniform prior for period,  $P$ , and time of transit minimum,  $\tau$ , between  $\pm 1$  day of that quoted by the NEA, and uniform priors for limb darkening coefficients  $q_1$  and  $q_2$  between 0 and 1. In total then, model  $\mathcal{P}$  had 7 free parameters. For model  $\mathcal{T}$ , the parameters are the same except the period is not fitted and simply fixed to the NEA MAP value. Similarly, there is no reference epoch, but instead a unique transit time for each epoch,  $\tau_i$ . This gives  $5 + N$  parameters for model  $\mathcal{T}$ , where  $N$  is the number of available epochs.

`MultiNest` substantially slows down beyond 20-25 free parameters, and thus if  $N \gg 1$ , this can lead to excessive computational times. KOIs-1355.01 and KOI-2992.01 have 27 and 16 available epochs respectively, sufficient that we chose to split the  $\mathcal{T}$  model up into 2 and 3 segments respectively, following Teachey & Kipping (2018). The downside of this is that the global shape parameters, such as  $b$  and  $\rho_*$ , are not self-consistent between the segments and not as precise as they could be, since they are conditioned upon only a fraction of the data. However, since our primary interest is the transit times themselves, which have little covariance with the other terms (Carter et al. 2008), this trade-off was considered acceptable.

#### 3.3 TTV analysis

The posteriors obtained in Section 3.2 may be used to define credible intervals for the transit times. We do so using the median and  $1\sigma$  quantiles.

Equipped with our independently derived transit times, we now proceed to evaluate if the candidate exomoon corridor signals persist in this cross check. The first step is to remove any possible outlier transit times.

Since have fit the data with a second model that explicitly assumes a linear ephemeris, we take the MAP ephemeris from model  $\mathcal{P}$  of each planet as a preliminary reference

ephemeris to define preliminary TTVs. From these, we calculate the standard deviation as a measure of the expected level of dispersion, against which we could look for outliers. However, even the standard deviation is itself a noisy estimate and so we add 5 standard deviations of the standard deviation onto this estimate to obtain a conservative maximum expected TTV deviance. Epochs where both components of the asymmetric uncertainty exceed this threshold were removed, since have weak constraining power and are likely driven by a partial/anomalous transit profile. We repeated this calculation on the H+16 transit times to produce a later fair comparison.

We next turn to repeating the periodogram exercise. Since our own transit times have asymmetric uncertainties, we modify our weighted linear least squares scheme to accommodate such asymmetries. The introduction of a Heaviside Theta function necessary to do this leads to a now non-linear problem, and thus the best-fit is obtained using a Nelder-Mead minimisation (Nelder & Mead 1965) of the  $\chi^2$  function. The periodogram uses a period grid defined in the same way as in Section 2.1, and similarly two models are regressed to the raw transit times (not the TTVs); a 2-parameter linear ephemeris model and a 4-parameter<sup>5</sup> linear ephemeris plus sinusoidal variation model.

### 3.4 Comparison to H+16 TTVs

Figures 4 & 5 present the TTVs of 10 of the 11 remaining KOIs (left panels). KOI-5825.01 was removed here since our own fits were unable to constrain the transit times at all, and every fit posterior returned the prior. The left-hand side figure panels also show the H+16 transit times for comparison in brown and slightly (artificially) offset to the right for clarity. Overlaid is the best-fitting sinusoidal signal from the periodogram search, for both data inputs.

This comparison reveals that in most cases there is good agreement concerning the locations of the best-fitting transit times, although exceptions certainly are present such as epoch 2 of KOI-1429.01, or epoch 11 of KOI-2296.01. Additionally, H+16 occasionally includes epochs that our own approach rejected, generally because the light curve quality was unacceptably poor; for example epochs 7 and 8 of KOI-1888.01 are present with H+16 but absent here. In that case, one can see that these epochs have a large impact on the retrieved sinusoid, leading to a much shorter period signal approaching the Nyquist rate.

Across the ensemble, the uncertainties are often quite distinct between our own measurements than that of H+16. Cross-matching epochs for which both data sets provide a transit time and ratioing their mean uncertainties, we find that our uncertainties are larger than that of H+16 in 65.6% of cases, with a median ratio of 1.09x and a mean ratio of 1.27x. The fact that H+16 has a tendency for smaller errors has an important consequence - the periodograms typically return higher significances than that derived using our own times. This is evident from the right panels of Figures 4 &

<sup>5</sup> Although four parameters are formally in the regression, recall that this regression sweeps across a grid of TTV periods too and we extract the maximum peak, hence defining an additional dimension of freedom.

5, where the H+16 periodogram peak exceeds that of our own in 9 out of 10 cases. As a result, although all 10 have  $\Delta\text{BIC} > 10$  using H+16 transit times, that number halves with the times derived here (KOIs-1429.01, 2992.01, 3678.01, 3762.01 & 5033.01). Some possible explanations for the discrepancies between H+16's transit times and that derived here are offered in Section 5.

### 3.5 Scrutinizing the candidacy of the remaining signals

The work presented here seeks to identify exomoon-like signatures using TTVs alone. Such an effort was previously made by Fox & Wiegert (2021), who claimed the existence of numerous new exomoon candidates by inspection of the H+16 TTV catalog. The claim was challenged in two independent papers, one which highlighted the implausible ability of many of these to retain large exomoons due to tidal evolution (Quarles, Li, & Rosario-Franco 2020) and another which showed that the KOIs failed a trifecta of tests designed to test to assess their candidacy (Kipping 2020). The latter paper also highlighted the importance of independently analysing the *Kepler* light curves, rather than adopting the H+16 catalog values as final. The three tests proposed serve as a benchmark standard in the current literature and thus we elected to adopt them here to scrutinise our remaining putative KOI signals. Afterall, if TTV exomoon candidates were killed using these tests in Kipping (2020), then any compelling signals claimed here should at least pass those same tests, which centre around three questions:

- Q1]** Are there statistically significant TTVs?
- Q2]** Is there a statistically significant periodic TTV?
- Q3]** Do the observations support a statistically significant non-zero moon mass?

### 3.6 Q1 - Significant TTVs?

At this point, the reader might suspect Q1 has already been convincingly answered. Afterall, the five KOIs remaining have been subject to a battery of significance tests already, including a complete re-analysis of the light curve data. However, all of these tests exploit the derived transit times, which are really a meta-product, rather than the photometry itself. Further, they frame the BIC in terms of raw degrees of freedom, rather than the physical degrees of freedom. To address this, Q1 takes the maximum likelihood from the photometric light curve fits of models  $\mathcal{P}$  and  $\mathcal{T}$  and compares those, rather than metrics based on the TTV meta-products. Following Kipping (2020) (see Section 3.1.4), the number of degrees of freedom is based upon the physical models that are needed to explain the data rather than that of the more ad-hoc case of simply assigning every epoch a new degree of freedom.

We applied this test to our 10 remaining KOIs, despite the fact 5 of them have already been shown to be spurious. We chose to do all 10 to provide some greater contextual examples of these tests in action. The results are shown in Table 1, where one can see that only 3 KOIs pass this simple test, KOIs-3678.01, 3762.01 and 5033.01. We note that all three of these are members of the five KOIs that survived our independent light curve analysis test in Section 3.4. KOI-3678.01 particularly stands out with an enor-

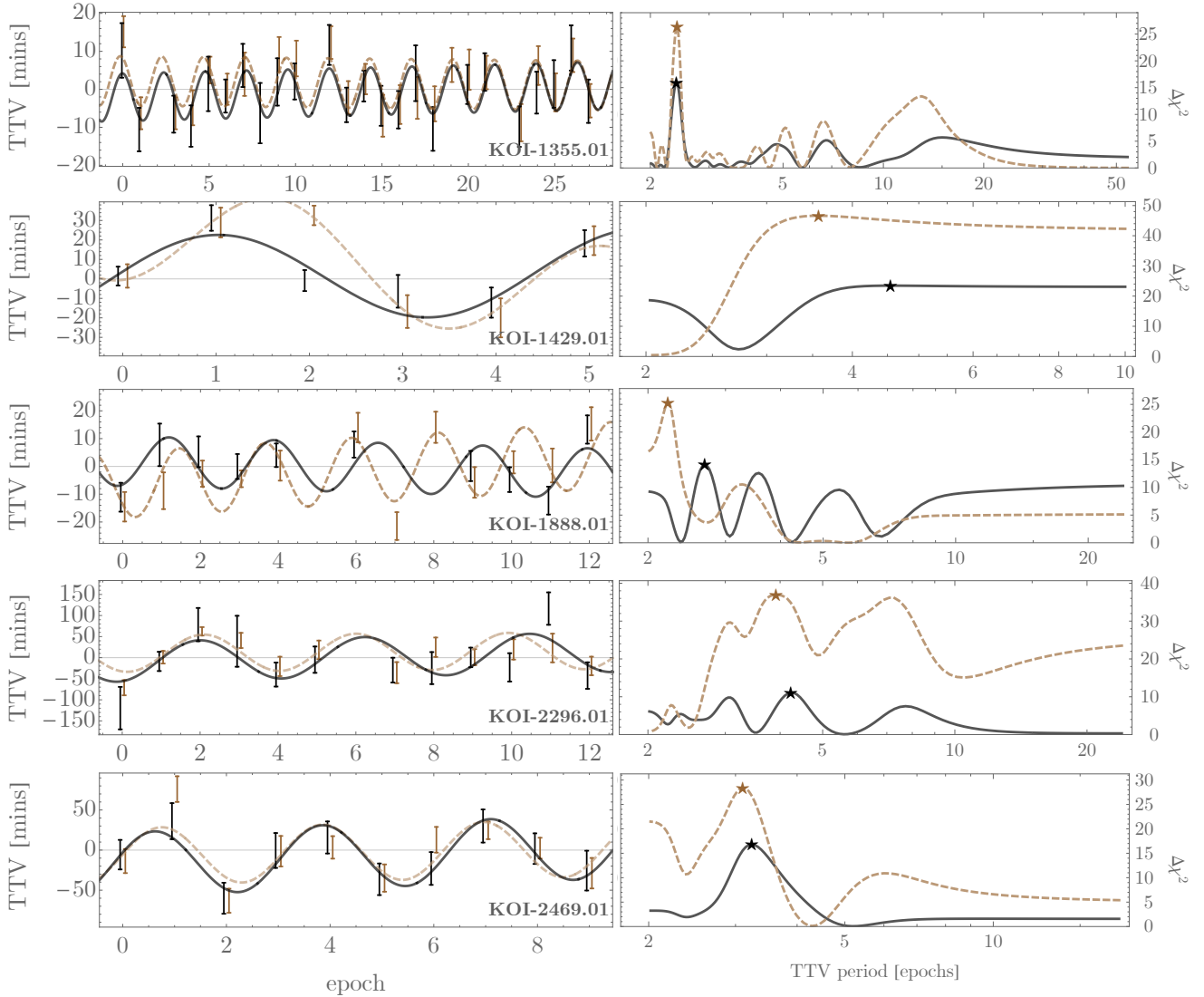


**Figure 4.** TTVs (left-panel) for 5 KOIs (labeled in the corners) ostensibly in the exomoon corridor to high significance from the H+16 catalog. Black points are those derived in this work from a full independent analysis, brown are those derived by H+16. With the same colours we overlay the best fitting sinusoid for each. Right panel shows the periodogram for each, where the best-fit (maximum likelihood) solution is highlighted with a star.

mous significance score of  $\Delta\text{BIC} = 207.9$ , which is particularly remarkable because the TTV amplitude is only 6.7 minutes (see Table 1).

### 3.7 Q2 - Significant periodic TTV?

In Q2, we follow the cross-validation tests of Kipping (2020) using the same 20% hold-out set (rounded to an integer number of epochs). Since  $0.2 \times n < 1.5$  for all  $n \leq 7$ , then KOIs with 7 or fewer useful epochs would only have a single epoch held-out, occurring for KOIs-1429.01, 3762.01 and 5033.01. In this test, the entire periodogram process is repeated a large number of times, which itself scans over a large number of frequencies. To maximise the efficiency of our cross-validation search then, the number of iterations of hold-out sets was set to  $\binom{n}{k}$ , where  $n$  is the number of epochs available and  $k$  is the size of the holdout set. In this way, we cycle

through all possible hold-out sets once. The only exception to this was KOI-1355.01, for which  $\binom{n}{k} = \binom{24}{5} = 42504$  which was simply too large to run in the time available. Instead, here, we simply did 425 as a 1% representative sample.

The cross-validation test essentially demands that the best-fitting model has useful predictive power, a basic expectation of a genuine physical model. Our criterion here is that  $> 50\%$  of the predictions using the sinusoidal TTV model must be superior to that of the linear ephemeris model, in a  $\chi^2$  sense. We are careful here to keep track of the asymmetric uncertainties in the transit times too in defining our  $\chi^2$  metric. The result is that four KOIs pass this test, KOI-1355.01, 2469.01, 3508.01 and 3678.01. At this point, only KOI-3678.01 now has a clean sweep of successful vetting tests.

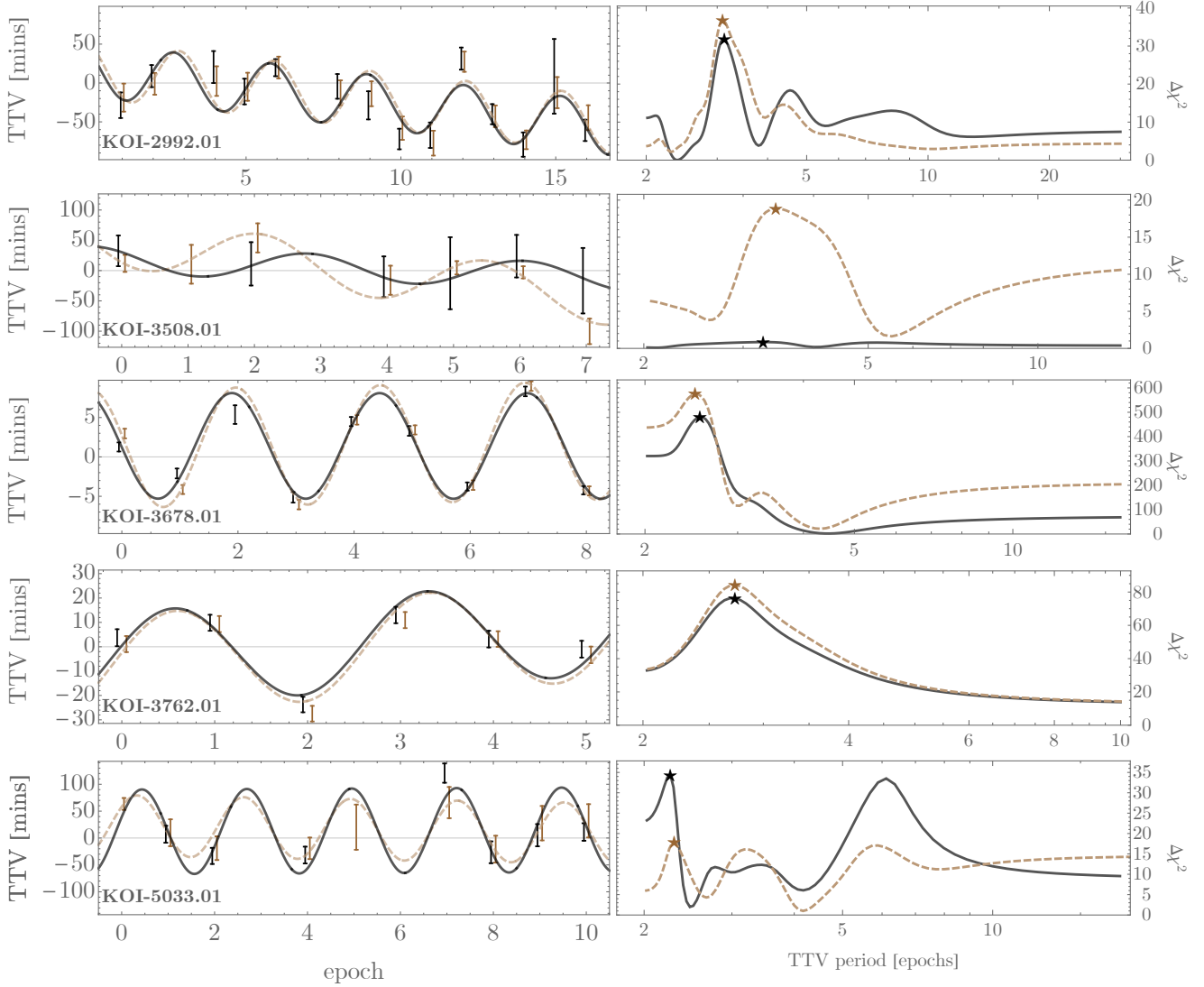


**Figure 5.** Same as Figure 4 for the other 5 KOIs.

### 3.8 Q3 - Significant non-zero moon mass?

As our third and final test, we fit (using `MultiNest`) a planet+moon photodynamical light curve model using LUNA (Kipping 2011) to the light curves. In this fit, we turn off the usual likelihood penalty function in our code that rejects any samples with unphysical satellite densities. This allows the fit to explore very low satellite masses without penalty and thus the moon mass posterior is able to peak at zero in cases where no evidence for a moon-like dynamical signature is found. We then assess the posterior density at zero with a Savage-Dickey ratio Dickey (1971), to evaluate the Bayes factor of a non-zero mass exomoon model against the null (zero mass signal), denoted as  $K_{\mathcal{M}:\mathcal{X}}$ . We consider a KOI to pass this test if  $K_{\mathcal{M}:\mathcal{X}} > 10$ , denoting “strong evidence” on the Kass & Raftery (1995) scale.

The major benefit of this test over simple sinusoidal signal check is that exomoon TTVs are not always strict sinusoids (Rodenbeck, Heller, & Gizon 2020). Moon acceleration during the transit can distort the shape of the signal

and thus invalidates the assumptions of the analytic TTV theory (which predicts a sinusoid). Two KOIs pass this final test, but of most relevancy is that KOI-3678.01 completes a clean sweep of successful tests with this final challenge. At this point, we are confident that KOI-3678.01 is a genuine TTV signature with a periodicity, amplitude and shape consistent with that of an exomoon. We discuss this object in more detail in the next section.

It is also worth remarking that amongst the other KOIs, KOI-3762.01 comes very close to a full sweep as well, failing only the cross-validation test. Looking at the TTVs shown in Figure 5, one can see that the signal is strongly dependent upon a single epoch, epoch #2 in the figure. That one point is down, as found by both our work and H+16. The importance of that single point, and the paucity of epochs here (just 6) makes this a challenging KOI to work with. On this basis, we encourage future transit timing observations of KOI-3762.01, as it’s unclear how robust our cross-validation results are in such a challenging case.

**Table 1.** List of the various test metrics applied to the 11 KOIs which appear to exhibit an exomoon corridor signal using the H+16 catalog. Columns 2-4 list a pair of numbers, the first as derived using H+16 transit time and the second using our own analysis. Columns 5-8 list the trifecta of higher-level TTV tests previously proposed by Kipping (2020).

KOI	$A_{\text{TTV}}$ (mins)	$P_{\text{TTV}}$ (epochs)	$\Delta \text{BIC}$	$\Delta \text{BIC}_{\text{physical}}$ [Q1]	% of good TTV predictions [Q2]	$\log K_{\mathcal{M}:\mathcal{X}}$ [Q3]
1355.01	{6.51, 6.26} [✓, ✓]	{2.41, 2.39} [✓, ✓]	{16.8, 6.4} [✓, X]	-11.3 [X]	(287/425 <sup>†</sup> ) 67.5% [✓]	-1.3 [X]
1429.01	{27.13, 21.98} [✓, ✓]	{3.57, 4.55} [✓, X]	{41.3, 18.1} [✓, ✓]	-8.3 [X]	(0/6) 0.0% [X]	0.1 [X]
1888.01	{11.87, 8.96} [✓, ✓]	{2.22, 2.69} [✓, ✓]	{25.3, 7.2} [✓, X]	-11.8 [X]	(5/45) 11.1% [X]	0.7 [X]
2296.01	{43.60, 47.20} [✓, ✓]	{3.91, 4.23} [✓, X]	{29.5, 3.6} [✓, X]	-14.2 [X]	(0/66) 0.0% [X]	-1.3 [X]
2469.01	{35.25, 39.75} [✓, ✓]	{3.10, 3.24} [✓, ✓]	{21.5, 9.9} [✓, X]	-14.1 [X]	(24/45) 53.3% [✓]	-1.1 [X]
2992.01	{36.40, 34.42} [✓, ✓]	{3.09, 3.13} [✓, ✓]	{28.9, 23.9} [✓, ✓]	+1.3 [X]	(89/364) 24.4% [X]	-0.2 [X]
3508.01	{41.36, 21.92} [✓, ✓]	{3.43, 3.26} [✓, ✓]	{13.1, -4.5} [✓, X]	-18.6 [X]	(5/6) 83.3% [✓]	-0.5 [X]
3678.01	{7.50, 6.70} [✓, ✓]	{2.49, 2.54} [✓, ✓]	{569.2, 474.2} [✓, ✓]	+207.9 [✓]	(35/36) 97.2% [✓]	33.8 [✓]
3762.01	{56.52, 19.57} [✓, ✓]	{2.73, 2.73} [✓, ✓]	{78.9, 70.9} [✓, ✓]	+13.4 [✓]	(0/6) 0.0% [X]	34.5 [✓]
5033.01	{56.52, 78.72} [✓, X]	{2.30, 2.26} [✓, ✓]	{11.2, 28.6} [✓, ✓]	+25.7 [✓]	(1/7) 14.3% [X]	-1.92 [X]

## 4 THE CASE OF KEPLER-1513B

### 4.1 System parameters

KOI-3678.01 emerges as the only TTV candidate from our analysis for which we can confidently determine it exhibits a significant exomoon-corridor TTV. We note that this object was previously validated as Kepler-1513b (Morton et al. 2016) and we will switch to this monicker in what follows. This does not mean no other *Kepler* candidates are in the corridor, since numerous filters applied in this work may have excluded them (e.g. multis were excluded and should also exhibit corridor signatures; Teachey 2021). An example of this would be Kepler-1625b, which only has 3 *Kepler* epochs from which no clear TTVs are evident, but inclusion of a fourth epoch from the Hubble Space Telescope reveals a significant TTV (Teachey & Kipping 2018) that appears consistent with the exomoon corridor despite the significant degeneracies of only having four epochs in hand (see Kipping 2021).

Although one of our filters in Section 2 screened for TTVs above the ceiling predicted due to an exomoon, leveraging the tidal theory of Barnes & O’Brien (2002), it is worth re-visiting the question as to how physically feasible it is for Kepler-1513b to have an exomoon. Afterall, it was through this argument that Quarles, Li, & Rosario-Franco (2020) questioned the existence of the purported exomoons claimed in Fox & Wiegert (2021), which also exclusively used TTVs. In order to address this, we first need a set of fundamental parameters for the star and planet, which is challenged by the fact there is no planetary mass measurement in the previous literature.

To tackle this, we first used the `isochrones` package (Morton 2015) to derive posterior samples for the star. The stellar atmospheric parameters are taken from P. Dalba (priv. comm.) using Keck HIRES and `SpecMatch` (Petigura 2015; ?), the parallax from *Gaia* DR3 (Gaia Collaboration et al. 2021), and the *Kepler* apparent magnitude is used to constrain the luminosity. This reveals the star to be a late G-type star, slightly sub-Solar, with the parameters listed in Table 2.

These posteriors samples are combined with those from the  $\mathcal{T}$  light curve fits (which recall account for TTVs) to produce physical parameters for the planet itself, which are also listed in Table 2. This reveals Kepler-1513b to be around 75% of a Jupiter-radius. Comparing to the empirical mass-radius relation of Chen & Kipping (2017), one can see that the planet is likely a sub-Jovian mass object, but could also plausibly be a massive, highly compressed brown dwarf. This is directly seen when we push the radius samples through `forecaster` (Chen & Kipping 2017) giving a bimodal mass prediction. RV observations using SOPHIE cannot detect Kepler-1513b’s mass, but they do constrain it to be  $<1.43 M_{\text{Jup}}$  to 99% confidence, thus putting pressure on the second mode. This fact, combined with the lower occurrence rate of more massive planets (Fulton et al. 2021) and the preference to not be overzealous in predicting large moons (which large planetary masses inevitably allow for) led us to completely exclude the second mode which delineates at  $178 M_{\oplus}$ . Since each radius sample has a corresponding and covariant forecasted mass sample, we are careful to apply this down-filtering to the entire joint posterior sam-

ples to maintain the correct covariance. This leaves us with a mass forecast of  $[14.8 M_{\oplus}, 125.6 M_{\oplus}]$  to 95.45% confidence.

### 4.2 Maximum stable exomoon mass

It is now possible to more rigorously revisit the Barnes & O’Brien (2002) tidal limits for moon masses. To do so, we use our joint posteriors including the truncated forecasted Chen & Kipping (2017) samples, the  $R-(k_{2p}/Q_p)$  relation of Teachey, Kipping, & Schmitt (2018), and plug them into to Equation (8) of Barnes & O’Brien (2002). The equation requires an assumed maximum stable moon orbital radius, which we here take to be 0.4895 for a prograde moon following Domingos, Winter, & Yokoyama (2006), and a lifetime, which we take to be 5 Gyr.

From this we obtain a maximum stable moon mass of  $4.4^{+13.4}_{-3.5} M_{\oplus}$ , with a  $2\sigma$  lower limit at  $0.32 M_{\oplus}$ . Accordingly, Kepler-1513b appears capable of supporting a potentially terrestrial mass exomoon for 5 Gyr.

### 4.3 Implied exomoon mass from the TTVs

We next turn to the implied exomoon mass, given the TTVs. Unfortunately, with a TTV signal alone, there is no way to uniquely determine the exomoon period (Kipping 2009a), which means in turn one cannot invert a TTV amplitude into an implied mass. Indeed, taking the TTV periodicity and the planetary period, and using Equation (11) of Kipping (2021), we identify 1260 possible satellite periods that are compatible with the TTV period and lie between 48.95% of the Hill sphere and a planet-grazing orbit ( $= 2\pi\sqrt{R_p^3/(GM_p)}$ ).

However, this minimum and maximum period range allows to at least evaluate the range of plausible moon masses needed to explain the TTVs. To rigorously achieve this though, we first need a posterior distribution for the TTV amplitude and period. From the 9 available epochs, we decided to drop one epoch with a partial transit, epoch #2 on Figure 5. Partial transits are challenging to work with but the fact that a large data gap occurs here potentially compromises our method marginalised detrending scheme. With the 8 remaining epochs, we used `MultiNest` to regress a sinusoid + linear ephemeris model and obtain posteriors samples, giving  $P_{\text{TTV}} = 2.556^{+0.018}_{-0.018}$  cycles and amplitude  $A_{\text{TTV}} = 6.95^{+0.32}_{-0.33}$  minutes.

Equipped with this, we solve for the required satellite mass at each joint posterior sample in the extreme limits of the widest allowed moon and the closest allowed moon orbit. Masses are calculated using the deterministic version of the `forecaster` code (Chen & Kipping 2017), as was used earlier in Section 2.3. In the case of the former, we find that the moon would need to be just  $0.0094^{+0.0040}_{-0.0031} M_{\oplus}$ , or  $0.76^{+0.33}_{-0.25} M_{\oplus}$  - this occurs at a satellite period of 27.11 days. For the closest-in moon, we formally find  $0.34^{+0.14}_{-0.11} M_{\oplus}$  (occurring at a 3.1 hour satellite period) but highlight this is almost certainly an underestimate. For TTVs periods shorter than the transit duration (10.9 hours), there is significant satellite acceleration during the transit that is not correctly accounted for in the theory of Kipping (2009a). Accordingly, all we can state with any confidence is that the putative

**Table 2.** Credible intervals for various parameters of interest for Kepler-1513b (KOI-3678.01).

Parameter	Definition	Credible Interval
<i>Observational stellar parameters</i>		
$K_p$	Kepler apparent magnitude	$12.888 \pm 0.100$
$T_{\text{eff}}$ (K)	Stellar effective temperature	$5491 \pm 100$
(M/H) (dex)	Stellar metallicity	$0.17 \pm 0.06$
$\log g$ (dex)	Stellar surface gravity	$4.46 \pm 0.10$
$\pi$ (mas)	Parallax	$2.8446 \pm 0.0134$
<i>Fundamental stellar parameters</i>		
$M_*$ ( $M_\odot$ )	Stellar mass	$0.943^{+0.038}_{-0.037}$
$R_*$ ( $R_\odot$ )	Stellar radius	$0.950^{+0.078}_{-0.055}$
$\rho_*$ ( $\text{kg m}^{-3}$ )	Stellar density	$1540^{+350}_{-340}$
$L_*$ ( $L_\odot$ )	Stellar luminosity	$0.74^{+0.15}_{-0.10}$
<i>Transit fit parameters</i>		
$R_P/R_*$	Ratio-of-radii	$0.07882^{+0.00036}_{-0.00022}$
$\rho_{*,\text{LC}}$ ( $\text{kg m}^{-3}$ )	Transit stellar density	$1304^{+21}_{-53}$
$b$	Impact parameter	$0.109^{+0.095}_{-0.075}$
$q_1$	Limb darkening parameter	$0.446^{+0.040}_{-0.039}$
$q_2$	Limb darkening parameter	$0.327^{+0.031}_{-0.028}$
<i>TTV fit parameters</i>		
$P_P$ (days)	Orbital period	$160.884435^{+0.000062}_{-0.000064}$
$\tau_0$ (BJD <sub>UTC</sub> -2,455,000)	Time of transit minimum	$110.50597^{+0.00032}_{-0.00031}$
$P_{\text{TTV}}$ (cycles)	TTV periodicity	$2.556^{+0.018}_{-0.018}$
$A_{\text{TTV}}$ (mins)	TTV amplitude	$6.95^{+0.32}_{-0.33}$
$\phi_{\text{TTV}}$ (rads)	TTV phase	$3.212^{+0.072}_{-0.074}$
<i>Estimated parameters</i>		
$M_{P,\text{forecaster}}$ ( $M_\oplus$ )	Forecasted (+truncated) planet mass	$48^{+35}_{-21}$
$M_{S,\text{max}}$ ( $M_\oplus$ )	Maximum stable moon mass	$4.4^{+13.4}_{-3.5}$
$M_{S,\text{TTV,min}}$ ( $M_\mathbb{C}$ )	Minimum implied moon mass from TTVs	$0.76^{+0.33}_{-0.25}$

moon is approximately Lunar mass or greater. This highlights the significant challenge of confirming such a moon photometrically, since the dip of such the smallest allowed satellite would correspond to  $\sim 7$  ppm. For comparison, the error on the combined phase-folded Kepler-1513b light curve is 34 ppm integrated over the transit duration timescale, making such a tiny moon wholly undetectable in direct transit.

## 5 DISCUSSION

### 5.1 Differences with H+16 work

In Section 3.4, we reported how the H+16 uncertainties are smaller than that of this work in 66% of cases, with a mean ratio of a 27% difference. The tendency for smaller errors in the H+16 catalog explains why periodograms from that data set typically return higher significances, leading to higher peaks in 9-out-of-10 cross-checked cases, as well as why so few of 11 initially identified exomoon corridor candidates survived independent analysis.

A basic question one might ask is - what explains the differences in transit times between our own work and that of H+16? There are many distinctions between the methodologies, any of which could contribute to the differences in the final product. H+16 use what we would consider to be variant of the **local** detrending method, using polynomials

but scoring them with  $p$ -values from  $\mathcal{F}$ -tests rather than the BIC, whereas we used a total of eight detrendings and then method marginalised the ensemble. Transit times were inferred with an iterative templating procedure in H+16, whereas here a global light curve model is regressed to the time series. The templating procedure certainly has the potential to underestimate uncertainties, since the template is treated as fixed during the transit time search, the error in the transit shape is not technically propagated into the timing error. Generally, this might be argued as reasonable since the time of transit minimum has negligible covariance to the other parameters according to the result of Carter et al. (2008). However, that analysis was for a idealised trapezoidal light curve with no limb darkening, and realistic light curves in general do exhibit covariances across all parameters, especially when working with sparse data, partial transits, integration time effects and curved transit profiles.

In conclusion, we cannot pin-point a single effect that could lead to these differences as there were simply too many methodology changes, but highlight the need to be cautious is working with the H+16 TTVs without independent checks.

### 5.2 And what of Kepler-1513b?

The purpose of this paper is to identify interesting exomoon-like TTV signals from a large ensemble, rather than to perform a detailed analysis of any single object. As a result, a

lot more can and should be done on Kepler-1513b to uncover its true nature.

We first recommend precise radial velocities to measure the planetary mass to confirm the planetary nature of the object and better constrain our moon stability/mass calculations that `forecaster` can achieve. Such observations could also identify additional planets in the system that could potentially explain the TTVs without the need for an exomoon.

Along similar lines, we have only here considered the exomoon hypothesis as a possible perturber, but a TTV inversion under the planet-planet hypothesis would reveal the plausibility of such a scenario. Such an inversion is highly challenging since the period of the putative planet is unknown and highly multi-modal. Nevertheless, such an analysis could at least identify a set of plausible alternative periods and interrogate their physical feasibility.

## ACKNOWLEDGMENTS

The authors thank Paul Dalba for graciously sharing his team's spectroscopic parameters ahead of publication. The authors would like to thank the anonymous referee for helpful comments that improved this paper. Some of the data used herein were obtained at the W. M. Keck Observatory, which is operated as a scientific partnership among the California Institute of Technology, the University of California, and NASA. The Observatory was made possible by the generous financial support of the W. M. Keck Foundation. The authors recognize and acknowledge the cultural role and reverence that the summit of Maunakea has within the indigenous Hawaiian community. We are deeply grateful to have the opportunity to use observations taken from this mountain. Resources supporting this work were provided by the NASA High-End Computing (HEC) Program through the NASA Advanced Supercomputing (NAS) Division at Ames Research Center for the production of the SPOC data products. This research has made use of the NASA Exoplanet Archive, which is operated by the California Institute of Technology, under contract with the National Aeronautics and Space Administration under the Exoplanet Exploration Program. This paper includes data collected by the Kepler Mission. Funding for the Kepler Mission is provided by the NASA Science Mission directorate. This work has made use of data from the European Space Agency (ESA) mission Gaia (<https://www.cosmos.esa.int/gaia>), processed by the Gaia Data Processing and Analysis Consortium (DPAC, <https://www.cosmos.esa.int/web/gaia/dpac/consortium>). Funding for the DPAC has been provided by national institutions, in particular the institutions participating in the Gaia Multilateral Agreement. D.K. and D.Y. acknowledge support from NASA Grant #80NSSC21K0960. This work was enabled thanks to supporters of the Cool Worlds Lab, including Mark Sloan, Douglas Daughaday, Andrew Jones, Elena West, Tristan Zajonc, Chuck Wolfred, Lasse Skov, Graeme Benson, Alex de Vaal, Mark Elliott, Stephen Lee, Zachary Danielson, Chad Souter, Marcus Gillette, Tina Jeffcoat, Jason Rockett, Scott Hannum, Tom Donkin, Andrew Schoen, Jacob Black, Reza Ramezankhani, Steven Marks, Gary Canterbury, Nicholas Gebben, Joseph Alexander, Mike Hedlund, Dhruv Bansal, Jonathan Sturm,

Rand Corporation, Leigh Deacon, Ryan Provost, Brynjolfur Sigurjonsson, Benjamin Paul Walford, Nicholas De Haan, Joseph Gillmer, Emerson Garland & Alexander Leishman.

## DATA AVAILABILITY

The code used and results generated by this work are made publicly available at [this URL](#).

## REFERENCES

- Agnor C. B., Hamilton D. P., 2006, *Natur*, 441, 192. doi:10.1038/nature04792
- Barnes J. W., O'Brien D. P., 2002, *ApJ*, 575, 1087. doi:10.1086/341477
- Berger T. A., Huber D., van Saders J. L., Gaidos E., Tayar J., Kraus A. L., 2020, *AJ*, 159, 280. doi:10.3847/1538-3881/159/6/280
- Canup R. M., Ward W. R., 2002, *AJ*, 124, 3404. doi:10.1086/344684
- Carter J. A., Yee J. C., Eastman J., Gaudi B. S., Winn J. N., 2008, *ApJ*, 689, 499. doi:10.1086/592321
- Chen J., Kipping D., 2017, *ApJ*, 834, 17. doi:10.3847/1538-4357/834/1/17
- Colquhoun D., 2014, *RSOS*, 1, 140216. doi:10.1098/rsos.140216
- Danby J. M. A., 1988, "Fundamentals of celestial mechanics". Willmann-Bell (North Chesterfield, Virginia, US)
- Dickey, J. M., 1971, *Ann. Math. Statist.* 42, 204
- Domingos R. C., Winter O. C., Yokoyama T., 2006, *MNRAS*, 373, 1227. doi:10.1111/j.1365-2966.2006.11104.x
- Feroz F., Hobson M. P., Bridges M., 2009, *MNRAS*, 398, 1601. doi:10.1111/j.1365-2966.2009.14548.x
- Fox C., Wiegert P., 2021, *MNRAS*, 501, 2378. doi:10.1093/mnras/staa3743
- Fulton B. J., Rosenthal L. J., Hirsch L. A., Isaacson H., Howard A. W., Dedrick C. M., Sherstyuk I. A., et al., 2021, *ApJS*, 255, 14. doi:10.3847/1538-4365/abfcc1
- Gaia Collaboration, Brown A. G. A., Vallenari A., Prusti T., de Bruijne J. H. J., Babusiaux C., Biermann M., et al., 2021, *A&A*, 649, A1. doi:10.1051/0004-6361/202039657
- Hadden S., Lithwick Y., 2014, *ApJ*, 787, 80. doi:10.1088/0004-637X/787/1/80
- Heller R., Rodenbeck K., Bruno G., 2019, *A&A*, 624, A95. doi:10.1051/0004-6361/201834913
- Holczer T., Mazeh T., Nachmani G., Jontof-Hutter D., Ford E. B., Fabrycky D., Ragozzine D., et al., 2016, *ApJS*, 225, 9. doi:10.3847/0067-0049/225/1/9 [H+16]
- Ioannidis P., Huber K. F., Schmitt J. H. M. M., 2016, *A&A*, 585, A72. doi:10.1051/0004-6361/201527184
- Kane M., Ragozzine D., Flowers X., Holczer T., Mazeh T., Relles H. M., 2019, *AJ*, 157, 171. doi:10.3847/1538-3881/ab0d91
- Kass, R. E. & Raftery, A. E., 1995, *Journal of the American Statistical Association*, 90, 773. doi:10.2307/2291091
- Kipping D. M., 2009a, *MNRAS*, 392, 181. doi:10.1111/j.1365-2966.2008.13999.x
- Kipping D. M., 2009b, *MNRAS*, 396, 1797. doi:10.1111/j.1365-2966.2009.14869.x
- Kipping D. M., 2010, *MNRAS*, 408, 1758. doi:10.1111/j.1365-2966.2010.17242.x
- Kipping D. M., 2011, *MNRAS*, 416, 689. doi:10.1111/j.1365-2966.2011.19086.x
- Kipping D. M., Bakos G. Á., Buchhave L., Nesvorný D., Schmitt A., 2012, *ApJ*, 750, 115. doi:10.1088/0004-637X/750/2/115
- Kipping D. M., 2013, *MNRAS*, 435, 2152. doi:10.1093/mnras/stt1435

- Kipping D., Teachey A., 2020, *SerAJ*, 201, 25.  
doi:10.2298/SAJ2001025K
- Kipping D., 2020, *ApJL*, 900, L44. doi:10.3847/2041-8213/abafa9
- Kipping D., 2021, *MNRAS*, 500, 1851.  
doi:10.1093/mnras/staa3398
- Kipping D., Bryson S., Burke C., Christiansen J., Hardegree-Ullman K., Quarles B., Hansen B., et al., 2022, *NatAs*, 6, 367. doi:10.1038/s41550-021-01539-1
- Kolmogorov, A. N., 1933, *Giornale dell'Istituto Italiano degli Attuari*, 4, 83.
- Kreidberg L., Luger R., Bedell M., 2019, *ApJL*, 877, L15.  
doi:10.3847/2041-8213/ab20c8
- Lomb N. R., 1976, *Ap&SS*, 39, 447. doi:10.1007/BF00648343
- Mandel K., Agol E., 2002, *ApJL*, 580, L171. doi:10.1086/345520
- Mazeh T., Nachmani G., Holczer T., Fabrycky D. C., Ford E. B., Sanchis-Ojeda R., Sokol G., et al., 2013, *ApJS*, 208, 16.  
doi:10.1088/0067-0049/208/2/16
- Morton T. D., Bryson S. T., Coughlin J. L., Rowe J. F., Ravichandran G., Petigura E. A., Haas M. R., et al., 2016, *ApJ*, 822, 86. doi:10.3847/0004-637X/822/2/86
- Morton T. D., 2015, *ascl.soft*. ascl:1503.010
- Nelder, J. A. & R. Mead, 1965, *Computer Journal*, 7, 308.  
doi:10.1093/comjnl/7.4.308
- Nyquist, H., 1928, *Trans. AIEE*, 47, 617
- Petigura E. A., 2015, *PhDT*
- Petigura E. A., Howard A. W., Marcy G. W., Johnson J. A., Isaacson H., Cargile P. A., Hebb L., et al., 2017, *AJ*, 154, 107.  
doi:10.3847/1538-3881/aa80de
- Quarles B., Li G., Rosario-Franco M., 2020, *ApJL*, 902, L20.  
doi:10.3847/2041-8213/abba36
- Daly, R. A., 1946, *PAPS*, 90, 104.
- Rodenbeck K., Heller R., Gizon L., 2020, *A&A*, 638, A43.  
doi:10.1051/0004-6361/202037550
- Rowe J. F., Bryson S. T., Marcy G. W., Lissauer J. J., Jontof-Hutter D., Mullally F., Gilliland R. L., et al., 2014, *ApJ*, 784, 45. doi:10.1088/0004-637X/784/1/45
- Rowe J. F., Thompson S. E., 2015, *arXiv*, arXiv:1504.00707
- Sartoretti P., Schneider J., 1999, *A&AS*, 134, 553.  
doi:10.1051/aas:1999148
- Santerne A., Moutou C., Tsantaki M., Bouchy F., Hébrard G., Adibekyan V., Almenara J.-M., et al., 2016, *A&A*, 587, A64.  
doi:10.1051/0004-6361/201527329
- Scargle J. D., 1982, *ApJ*, 263, 835. doi:10.1086/160554
- Schwarz G., 1978, *AnSta*, 6, 461. doi:10.1214-aos/1176344136
- Smirnov, N., 1948, *Annals of Mathematical Statistics*, 19, 279.  
doi:10.1214/aoms/1177730256.
- Teachey A., Kipping D. M., Schmitt A. R., 2018, *AJ*, 155, 36.  
doi:10.3847/1538-3881/aa93f2
- Teachey A., Kipping D. M., Schmitt A. R., 2018, *AJ*, 155, 36.  
doi:10.3847/1538-3881/aa93f2
- Teachey A., Kipping D. M., 2018, *SciA*, 4, eaav1784.  
doi:10.1126/sciadv.aav1784
- Teachey A., 2021, *MNRAS*, 506, 2104.  
doi:10.1093/mnras/stab1840
- Thompson S. E., Coughlin J. L., Hoffman K., Mullally F., Christiansen J. L., Burke C. J., Bryson S., et al., 2018, *ApJS*, 235, 38. doi:10.3847/1538-4365/aab4f9
- VanderPlas J. T., 2018, *ApJS*, 236, 16. doi:10.3847/1538-4365/aab766
- Wasserstein, R. L. & Lazar N. A., 2016, *The American Statistician*, 70, 129–133. doi:10.1080/00031305.2016.1154108

This paper has been typeset from a *T<sub>E</sub>X/L<sub>A</sub>T<sub>E</sub>X* file prepared by the author.